Available online at www.sciencedirect.com
ScienceDirect
PERGAMON
Acta Astronautica 65 (2009) 112–122
ACTA ASTRONAUTICA
www.elsevier.com/locate/actaastro

Adaptive control for satellite formation flying under thrust misalignment

Hyung-Chul Lim[a,*], Hyochoong Bang[b]

[a] *Korea Astronomy and Space Science Institute, Daejeon 305-348, Republic of Korea*
[b] *Department of Aerospace Engineering, Korea Advanced Institute of Science and Technology, Daejeon 305-701, Republic of Korea*

Received 10 October 2008; received in revised form 18 December 2008; accepted 8 January 2009
Available online 3 March 2009

Abstract

Satellite formation flying requires precise control of relative positioning under external disturbances and parameter uncertainties. Since thrust magnitude error and misalignment are not negligible in the electric propulsion system, they should be considered in satellite formation flying to meet mission requirements. In this paper, an adaptive control approach combined with backstepping technique is developed by using Lyapunov control design approach for the relative position tracking problem of satellite formation flying in the presence of thrust misalignment uncertainty and disturbances. The proposed controller guarantees global asymptotic convergence for position and velocity tracking error to ensure desired performance during the satellite formation flying mission.

Keywords: Satellite formation flying; Adaptive backstepping control; Thrust misalignment

1. Introduction

Recently, satellite formation flying (SFF) has been a topic of significant research interest in aerospace society because it provides potential benefits compared to a single large spacecraft: low cost for launch and mass production, larger aperture size, greater launch flexibility, higher system reliability and easier expandability. The current literature related to SFF largely focus on the control problem of relative position based on linear and nonlinear dynamic models. Control designs based on the linearized dynamics known as Hill's equations [1] require extra fuel consumption and may not guarantee successful formation flying performance with long duration and large separation between satellites. So some nonlinear control laws have been presented for the tracking problem of SFF, which include full-nonlinear dynamics, external disturbances and parameter uncertainty. Queiroz [2] developed a nonlinear adaptive control law for the relative position tracking of multiple satellites. Gurfil [3] studied a nonlinear adaptive neural control methodology for deep-space SFF. Pongvthithum [4] designed a tracking control law using the universal adaptive control technique. Majority of nonlinear control approaches for SFF missions are based on full state feedback controllers which assume that both position and velocity sensors are available. On the other hand, Wong [5] designed an adaptive output feedback tracking control in the absence of velocity measurement.

Some unknown parameters may appear in the relative dynamics of SFF, which include mass, thrust magnitude error, and misalignment. Satellite mass has been handled as a constant uncertainty in the control problem of SFF using an adaptive control scheme, even though the mass can change slightly due to fuel consumption.

* Corresponding author.
E-mail address: hclim@kasi.re.kr (H.-C. Lim).

0094-5765/$ - see front matter © 2009 Elsevier Ltd. All rights reserved.
doi:10.1016/j.actaastro.2009.01.022

Lim [6] developed an adaptive backstepping control law considering the ratio of thrust magnitude error as an unknown parameter under the assumption that thrust magnitude error is proportional to its magnitude. Adaptive backstepping technique has been considered as a powerful tool for stabilizing nonlinear systems under parameter uncertainties both for tracking and regulation problems. This technique introduced by Kanellakopoulos [7] for feedback linearizable systems has been extended to a wide class of nonlinear systems by many researchers. In addition, some methods have been proposed to improve the robustness of adaptive controllers by adding a leakage term such as switching σ-modification [8] and e_1-modification [9] to the parameter update law or using the projection operator [10].

The practical implementation of SFF depends on accurate control of the relative position and orientation among satellites, which requires low thrust and long lifetime for the propulsion system. The electric propulsion system provides high control accuracy and long lifetime so that it is a suitable candidate for precise relative positioning tasks such as SSF. Qingsong [11] and Hui [12] used low thrust for formation keeping by applying fuzzy control and formation maneuvering with sliding mode control approach. For an ion thruster belonging to an electric propulsion system, thrust magnitude error and misalignment are not negligible during orbit maneuver. It has been found, in calibration simulations for an ion thruster, that thrust magnitude error can be reduced to an accuracy of 1.2% with a maximum absolute error of 0.5 mN and misalignment from 0.5° to 5° [13]. Thus, thrust error including misalignment can be a serious problem in orbit control missions with high accuracy requirement, even though thrust error is calibrated through the process of orbit and attitude maneuvers prior to carrying out designed missions.

In comparison to the previous works, the contributions of this paper can be summarized as follows: a thrust error model is developed for a single thruster with misalignment, and an adaptive backstepping control law is also developed by using the Lyapunov-based control design approach to solve the relative position tracking problem of SFF under the presence of thrust misalignment and disturbances. Thrust misalignment is considered as an unknown parameter and updated through a parameter update law in the proposed control law. In addition, an approach for computing the control input is addressed because the control input cannot be evaluated explicitly from the control law developed. The proposed control law guarantees global asymptotic convergence for the position and velocity tracking error to ensure desired performance during the SSF mission.

2. System model

2.1. Relative dynamics

A rotating local–vertical–local–horizontal (LVLH) coordinate frame is used to describe the relative motion dynamics with respect to a leader satellite. As shown in Fig. 1 (left), y-axis points to the radial direction, z-axis is perpendicular to the orbital plane and points to the direction of orbital angular momentum vector. Finally, x-axis points to the opposite along-track direction. In general, the Clohessy–Wiltshire equation defined in the LVLH frame is utilized to describe the relative motion and control strategies between neighboring satellites under some assumptions, and usually called Hill's equations. However, non-linear relative dynamics is employed to design an adaptive backstepping controller in this study.

The relative motion dynamics of the follower satellite in the LVLH frame is described as the following set of nonlinear differential equations [14]:

$$\begin{aligned}
&\ddot{x} - 2\omega\dot{y} - \dot{\omega}y - \omega^2 x + \frac{\mu x}{\|\mathbf{R}+\mathbf{x}_1\|^3} - \frac{F_{lx}}{m_l} - d_x = \frac{F_x}{m_f}\\
&\ddot{y} + 2\omega\dot{x} + \dot{\omega}x - \omega^2 y + \frac{\mu(y+r)}{\|\mathbf{R}+\mathbf{x}_1\|^3} - \frac{\mu r}{\|R\|^3} - \frac{F_{ly}}{m_l} - d_y = \frac{F_y}{m_f}\\
&\ddot{z} + \frac{\mu z}{\|\mathbf{R}+\mathbf{x}_1\|^3} - \frac{F_{lz}}{m_l} - d_z = \frac{F_z}{m_f}
\end{aligned} \tag{1}$$

where $\mathbf{R} = [0, r, 0]^{\mathrm{T}}$ denotes the position vector of the leader satellite in the inertial coordinate system which is attached to the center of the Earth; $\mathbf{x}_1 = [x, y, z]^{\mathrm{T}}$ represents the relative position vector of the follower satellite in the LVLH frame whose origin is at the center of the leader satellite; $\mathbf{F}_l = [F_{lx}, F_{ly}, F_{lz}]^{\mathrm{T}}$ and $\mathbf{F} = [F_x, F_y, F_z]^{\mathrm{T}}$ are thrust forces of the leader and the follower satellites, respectively; m_l and m_f refer to the masses of the leader and the follower satellites, respectively; $\mathbf{d} = [d_x, d_y, d_z]^{\mathrm{T}}$ represents unknown time-varying disturbance caused by the Earth's oblateness including J_2 perturbation of the second spherical harmonic in the Earth's gravity field, solar radiation pressure, atmospheric drag, third body gravity and electromagnetic force; μ is the Earth's gravitational constant; ω denotes the orbital angular velocity of the

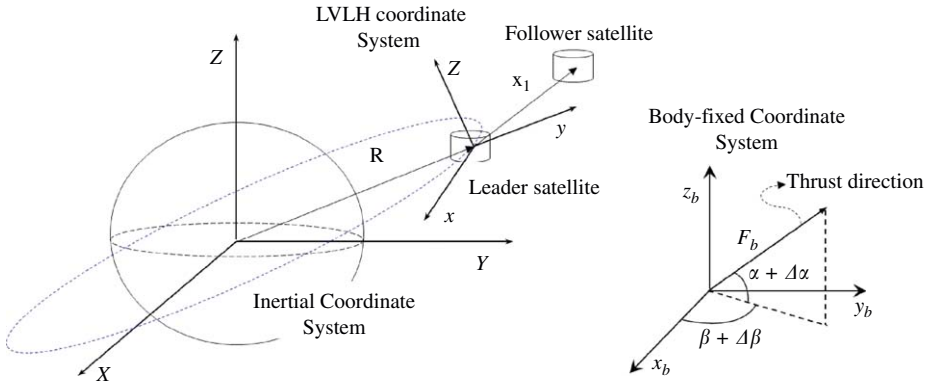

Fig. 1. Schematic representation of the SFF system (left) and thruster error (right).

leader satellite, whose time derivative is zero for a circular orbit and nonzero for an eccentric orbit.

If the leader is free of thrust maneuver as a virtual reference, then Eq. (1) can be simplified into the following equations:

$$\dot{\mathbf{x}}_1 = \mathbf{x}_2$$
$$\dot{\mathbf{x}}_2 = f(\mathbf{x}_1, \mathbf{x}_2) + \mathbf{d} + \frac{\mathbf{F}}{m_f} \tag{2}$$

where

$$f(\mathbf{x}_1, \mathbf{x}_2) = \begin{bmatrix} 2\omega\dot{y} + \dot{\omega}y + \omega^2 x - \dfrac{\mu x}{\|\mathbf{R}+\mathbf{x}_1\|^3} \\ -2\omega\dot{x} - \dot{\omega}x + \omega^2 y - \dfrac{\mu(y+r)}{\|\mathbf{R}+\mathbf{x}_1\|^3} + \dfrac{\mu r}{\|\mathbf{R}\|^3} \\ -\dfrac{\mu z}{\|\mathbf{R}+\mathbf{x}_1\|^3} \end{bmatrix}$$

and $\mathbf{x}_2 \in R^3$ denotes the velocity of the follower satellite in the LVLH frame.

2.2. Thrust error model

In this section, the thrust error of the propulsion system such as ion thruster is mathematically modeled for a satellite with a single thruster, which includes thrust magnitude error and misalignment. Referring to Fig. 1 (right), it is assumed that the thruster is tilted over nominal thrust direction with small constant angles, $\Delta\alpha$ and $\Delta\beta$, and the thrust is always acting at the center of the mass of the satellite. The real thrust force with magnitude error and misalignment is expressed as the sum of nominal and thrust error terms in the body frame

$$\mathbf{F}_b = \mathbf{F}_b^* + \Delta\mathbf{F}_b = (T_m + \Delta T_m) \begin{bmatrix} \cos(\alpha+\Delta\alpha)\cos(\beta+\Delta\beta) \\ \cos(\alpha+\Delta\alpha)\sin(\beta+\Delta\beta) \\ \sin(\alpha+\Delta\alpha) \end{bmatrix} \tag{3}$$

where $\mathbf{F}_b^* \in R^3$ and $\Delta\mathbf{F}_b \in R^3$ denote nominal force and thrust error caused by magnitude error and misalignment of thruster, respectively; T_m and ΔT_m represent the nominal and error of thrust magnitude, respectively. Thrust magnitude error can be assumed as $\Delta T_m = \kappa(t) \cdot T_m$ by introducing a small time-varying function, $\kappa(t)$ which is a small random variable in practical problems. In addition, the following relationships are adopted to approximate Eq. (3):

$$\cos\Delta\alpha \approx \cos\Delta\beta \approx 1$$
$$\sin\Delta\alpha \approx \Delta\alpha, \sin\Delta\beta \approx \Delta\beta$$
$$\Delta\alpha \cdot \Delta\beta \approx \Delta\alpha \cdot \kappa(t) \approx \Delta\beta \cdot \kappa(t) \approx 0 \tag{4}$$

By some algebraic manipulation with Eq. (4), Eq. (3) can be rewritten as

$$\begin{aligned} \mathbf{F}_b &\approx (T_m + \Delta T_m) \begin{bmatrix} c\alpha \cdot c\beta \\ c\alpha \cdot s\beta \\ s\alpha \end{bmatrix} \\ &\quad + \Delta\alpha(T_m + \Delta T_m) \begin{bmatrix} -s\alpha \cdot c\beta \\ -s\alpha \cdot s\beta \\ c\alpha \end{bmatrix} \\ &\quad + \Delta\beta(T_m + \Delta T_m) \begin{bmatrix} -c\alpha \cdot s\beta \\ c\alpha \cdot c\beta \\ 0 \end{bmatrix} \\ &\approx T_m \begin{bmatrix} c\alpha \cdot c\beta \\ c\alpha \cdot s\beta \\ s\alpha \end{bmatrix} + T_m \begin{bmatrix} -c\alpha \cdot s\beta & -s\alpha \cdot c\beta \\ c\alpha \cdot c\beta & -s\alpha \cdot s\beta \\ 0 & c\alpha \end{bmatrix} \begin{bmatrix} \Delta\beta \\ \Delta\alpha \end{bmatrix} \\ &\quad + \kappa(t) T_m \begin{bmatrix} c\alpha \cdot c\beta \\ c\alpha \cdot s\beta \\ s\alpha \end{bmatrix} \end{aligned} \tag{5}$$

where $c(\cdot)$ and $s(\cdot)$ represent cosine and sine functions, respectively. In the second equation of Eq. (5), the first term corresponds to the nominal thrust force, and the

second one to the thrust error caused by misalignment, and the third one to thrust magnitude error.

Two rotation matrices are introduced to describe the desired thrust force in the LVLH frame, $C_B^L \in R^{3\times3}$ and $C_R \in R^{3\times3}$. C_B^L represents the matrix to transform the thrust vector in the body frame to the LVLH frame, whereas C_R denotes the matrix to rotate a thruster to the desired direction in the LVLH frame and is realized by attitude control in practical implementation. Then the thrust dynamics in the LVLH frame can be rewritten as

$$\begin{aligned}\mathbf{F} &= C_R \cdot C_B^L \cdot \mathbf{F}_b = C_{LB}^R \cdot (\mathbf{F}_b^* + \Delta\mathbf{F}_b)\\ &= \mathbf{u} + T_m \cdot C_{LB}^R \cdot G \cdot \theta + \kappa(t) T_m \cdot C_{LB}^R \cdot \hat{\boldsymbol{\xi}}\end{aligned} \tag{6}$$

where

$$\mathbf{u} = T_m \cdot C_{LB}^R \cdot \hat{\boldsymbol{\xi}}, \quad C_{LB}^R = C_R \cdot C_B^L$$

$$\hat{\boldsymbol{\xi}} = \begin{bmatrix} c\alpha \cdot c\beta \\ c\alpha \cdot s\beta \\ s\alpha \end{bmatrix}, \quad \theta = \begin{bmatrix} \Delta\beta \\ \Delta\alpha \end{bmatrix},$$

$$G = \begin{bmatrix} -c\alpha \cdot s\beta & -s\alpha \cdot c\beta \\ c\alpha \cdot c\beta & -s\alpha \cdot s\beta \\ 0 & c\alpha \end{bmatrix}$$

$\hat{\boldsymbol{\xi}} \in R^3$ is a constant unit vector of direction cosines representing thrust direction in the body frame, the nominal thrust force, $\mathbf{u}=[u_x, u_y, u_z]^{\mathrm{T}}$ in Eq. (6) is computed from an adaptive backstepping control law, and the unknown parameter $\theta \in R^2$ is estimated from a parameter update law in this study. According to the definition of Eq. (6), the nominal thrust force can be calculated directly from the thrust magnitude T_m and the rotation matrix of thrust C_{LB}^R in the LVLH frame. Note that the thrust force $\mathbf{F}$ is applied to nonlinear relative dynamics of Eq. (2) because it contains the nominal thrust force and also thrust error including thrust magnitude error and misalignment, but the actual control input through the control law is the nominal thrust force $\mathbf{u}$, not the thrust force $\mathbf{F}$. This topic will be elaborated in the next section. If thrust magnitude error ΔT_m is proportional to thrust magnitude, i.e., $\Delta T_m = \kappa \cdot T_m$ for which κ is a constant, then the thrust dynamics of Eq. (6) can be expressed as

$$\mathbf{F} = \mathbf{u} + T_m \cdot C_{LB}^R \cdot G' \cdot \theta' \tag{7}$$

where

$$\theta' = \begin{bmatrix} \kappa \\ \Delta\beta \\ \Delta\alpha \end{bmatrix}, \quad G' = \begin{bmatrix} c\alpha \cdot c\beta & -c\alpha \cdot s\beta & -s\alpha \cdot c\beta \\ c\alpha \cdot s\beta & c\alpha \cdot c\beta & -s\alpha \cdot s\beta \\ s\alpha & 0 & c\alpha \end{bmatrix}$$

3. Adaptive backstepping controller design

3.1. Control and parameter update law design

In this section, control and parameter update laws are designed for the tracking problem of SFF with thrust misalignment using an adaptive backstepping technique. We make two assumptions on the nonlinear relative dynamics; disturbance applied to the follower satellite is bounded such that $|\mathbf{D}_i| \leqslant \bar{\mathrm{D}}$ in which thrust magnitude error is also included, and the misalignment vector $\theta = [\Delta\beta, \Delta\alpha]^{\mathrm{T}}$ is unknown, but lies within a known sphere, i.e., $\|\theta\| \leqslant M_\theta$. After substituting the thrust error model of Eq. (6) into the relative dynamics of Eq. (2), the nonlinear relative dynamics can be expressed as

$$\begin{aligned}\dot{\mathbf{x}}_1 &= \mathbf{x}_2\\ \dot{\mathbf{x}}_2 &= f(\mathbf{x}_1, \mathbf{x}_2) + \frac{\mathbf{u}}{m_f} + \frac{T_m}{m_f} \cdot C_{LB}^R \cdot G \cdot \theta + \mathbf{d}(t)\\ &\quad + \frac{T_m}{m_f} \kappa(t) \cdot C_{LB}^R \cdot \hat{\boldsymbol{\xi}}\\ &= f(\mathbf{x}_1, \mathbf{x}_2) + \frac{\mathbf{u}}{m_f} + H(t)\theta + \mathbf{D}(t)\end{aligned} \tag{8}$$

where

$$H(t) = \frac{T_m}{m_f} \cdot C_{LB}^R \cdot G,$$

$$\mathbf{D}(t) = \mathbf{d}(t) + \frac{T_m}{m_f} \kappa(t) \cdot C_{LB}^R \cdot \hat{\boldsymbol{\xi}}$$

Note that $H(t) \in R^{3\times2}$ is a time-varying matrix including thrust magnitude T_m and the rotation matrix C_{LB}^R.

Given a desired trajectory $\mathbf{x}_d \in R^3$ for the follower satellite with respect to the leader, the primary objective is to design a control law such that the follower satellite tracks the desired trajectory well under thrust misalignment and disturbances. It is assumed that $\mathbf{x}_1$ and $\mathbf{x}_2$ are measurable, and $\mathbf{x}_d$ is a known bounded signal such that $\dot{\mathbf{x}}_d$ and $\ddot{\mathbf{x}}_d$ are bounded and differentiable. The design procedure of an adaptive backstepping control is described in the following three steps.

Step 1: For the position tracking problem, a tracking error is defined as $\mathbf{z}_1 = \mathbf{x}_1 - \mathbf{x}_d$, and the first Lyapunov function candidate is proposed as

$$V_1(\mathbf{z}_1) = \tfrac{1}{2}\mathbf{z}_1^{\mathrm{T}} \Lambda_1 \mathbf{z}_1 \tag{9}$$

According to the typical backstepping design technique [10], a corresponding stabilizing function is defined as $\boldsymbol{\alpha}_1 = -C_1\mathbf{z}_1$. $\Lambda_1 \in R^{3\times3}$ and $C_1 \in R^{3\times3}$ are constant, diagonal and positive-definite design matrices. With the

new error variable introduced as $\mathbf{z}_2 = \mathbf{x}_2 - \dot{\mathbf{x}}_d - \boldsymbol{\alpha}_1$, the time derivative of V_1 is given by

$$\dot{V}_1 = -\mathbf{z}_1^{\mathrm{T}} \Lambda_1 C_1 \mathbf{z}_1 + \mathbf{z}_1^{\mathrm{T}} \Lambda_1 \mathbf{z}_2 \tag{10}$$

Step 2: By using these new variables, the nonlinear system Eq. (8) can be rewritten as

$$\begin{aligned} \dot{\mathbf{z}}_1 &= \mathbf{z}_2 - C_1 \mathbf{z}_1 \\ \dot{\mathbf{z}}_2 &= f + \mathbf{D} + \frac{\mathbf{u}}{m_f} + H\theta - \ddot{\mathbf{x}}_d \\ &\quad + C_1(\mathbf{z}_2 - C_1 \mathbf{z}_1) \end{aligned} \tag{11}$$

The second Lyapunov function candidate is chosen as

$$V_2(\mathbf{z}_1, \mathbf{z}_1) = V_1(\mathbf{z}_1) + \tfrac{1}{2}\mathbf{z}_2^{\mathrm{T}} \Lambda_2 \mathbf{z}_2 \tag{12}$$

where $\Lambda_2 \in R^{3\times 3}$ is also a constant, diagonal and positive-definite design matrix. The derivative of V_2 can be derived as

$$\begin{aligned} \dot{V}_2 = & -\mathbf{z}_1^{\mathrm{T}} \Lambda_1 C_1 \mathbf{z}_1 + \mathbf{z}_2^{\mathrm{T}} \Lambda_2 \left[f + \mathbf{D} + \frac{\mathbf{u}}{m_f} + H\theta - \ddot{\mathbf{x}}_d \right. \\ & \left. + C_1(\mathbf{z}_2 - C_1 \mathbf{z}_1) + \Lambda_2^{-1} \Lambda_1 \mathbf{z}_1 \right] \end{aligned} \tag{13}$$

Step 3: Since the thrust misalignment vector θ is unknown in the square bracket of Eq. (13), an adaptive law is proposed to accommodate the uncertainty of thrust misalignment. The estimate error of thrust misalignment is defined as $\tilde{\theta} = \theta - \hat{\theta}$ in which the estimate vector $\hat{\theta}$ is updated using an adaptation algorithm. The third Lyapunov function candidate is chosen as

$$V_3(\mathbf{z}_1, \mathbf{z}_2, \tilde{\theta}) = V_2(\mathbf{z}_1, \mathbf{z}_2) + \tfrac{1}{2}\tilde{\theta}^{\mathrm{T}} \Gamma^{-1} \tilde{\theta} \tag{14}$$

where $\Gamma \in R^{2\times 2}$ is a constant, diagonal and positive-definite design matrix. The time derivative of V_3 is given by

$$\begin{aligned} \dot{V}_3 = & -\mathbf{z}_1^{\mathrm{T}} \Lambda_1 C_1 \mathbf{z}_1 + \mathbf{z}_2^{\mathrm{T}} \Lambda_2 \\ & \times \left[f + \mathbf{D} + \frac{\mathbf{u}}{m_f} + H\hat{\theta} - \ddot{\mathbf{x}}_d + C_1(\mathbf{z}_2 - C_1 \mathbf{z}_1) \right. \\ & \left. + \Lambda_2^{-1} \Lambda_1 \mathbf{z}_1 \right] + (\mathbf{z}_2^{\mathrm{T}} \Lambda_2 H - \dot{\hat{\theta}}^{\mathrm{T}} \Gamma^{-1}) \tilde{\theta} \end{aligned} \tag{15}$$

According to Eq. (15), an adaptive backstepping control law and a parameter update law are proposed as Eqs. (16) and (17) such that the time derivative of V_3 becomes non-positive

$$\begin{aligned} \mathbf{u} = & m_f(-C_2 \mathbf{z}_2 - f - \bar{\mathrm{D}}\,\mathrm{Sgn}(\mathbf{z}_2) + \ddot{\mathbf{x}}_d \\ & - C_1(\mathbf{z}_2 - C_1 \mathbf{z}_1) - \Lambda_2^{-1} \Lambda_1 \mathbf{z}_1) - m_f H \hat{\theta} \end{aligned} \tag{16}$$

$$\dot{\hat{\theta}} = \Gamma H^{\mathrm{T}} \Lambda_2 \mathbf{z}_2 + \Gamma \sigma_\theta(\hat{\theta}) \hat{\theta} \tag{17}$$

where $C_2 \in R^{3\times 3}$ is a constant, diagonal and positive-definite design matrix, and $\mathrm{Sgn}(\boldsymbol{\zeta})$ represents a *signum* function defined as

$$\begin{aligned} &\mathrm{Sgn}(\boldsymbol{\zeta}) = [\mathrm{sgn}(\zeta_1), \mathrm{sgn}(\zeta_2), \ldots, \mathrm{sgn}(\zeta_m)]^{\mathrm{T}}, \\ &\forall \boldsymbol{\zeta} = [\zeta_1, \zeta_2, \ldots, \zeta_m]^{\mathrm{T}} \end{aligned} \tag{18}$$

In the parameter update law (Eq. (17)), a switching σ-modification [8] strategy is added to prevent parameter drift with the following definition:

$$\sigma_\theta(\hat{\theta}) = \begin{cases} 0 & \text{if } \|\hat{\theta}\| \leqslant M_\theta \\ \bar{\sigma}_\theta \left(\dfrac{\|\hat{\theta}\|}{M_\theta} - 1 \right) & \text{if } M_\theta \leqslant \|\hat{\theta}\| \leqslant 2M_\theta \\ \bar{\sigma}_\theta & \text{if } \|\hat{\theta}\| \geqslant 2M_\theta \end{cases} \tag{19}$$

where $\bar{\sigma}_\theta$ is a positive constant and scalar design parameter. If $\|\hat{\theta}\| \leqslant M_\theta$, then $\sigma(\hat{\theta}) = 0$ from its definition. On the contrary, if $\|\hat{\theta}\| > M_\theta$, then $(\|\theta\|\,\|\hat{\theta}\| - \|\hat{\theta}\|^2) < 0$. By using such properties, the second term of Eq. (17) is derived, which is useful in the closed-loop system stability analysis

$$\begin{aligned} \sigma(\hat{\theta})\tilde{\theta}^{\mathrm{T}}\hat{\theta} &= \sigma(\hat{\theta})(\theta - \hat{\theta})^{\mathrm{T}}\hat{\theta} = \sigma(\hat{\theta})(\theta^{\mathrm{T}}\hat{\theta} - \|\hat{\theta}\|^2) \\ &\leqslant \bar{\sigma}(\|\theta\|\,\|\hat{\theta}\| - \|\hat{\theta}\|^2) \\ &\leqslant 0 \end{aligned} \tag{20}$$

3.2. Stability analysis

The proposed adaptive control laws described by Eqs. (16) and (17) guarantee global asymptotic convergence for the position and velocity tracking errors. After substituting the control law of Eq. (16) and the parameter update law of Eq. (17) into Eq. (15), and then applying the property of the switching σ-modification in Eq. (20), we arrive at

$$\begin{aligned} \dot{V}_3 = & -\mathbf{z}_1^{\mathrm{T}} \Lambda_1 C_1 \mathbf{z}_1 - \mathbf{z}_2^{\mathrm{T}} \Lambda_2 C_2 \mathbf{z}_2 \\ & + \mathbf{z}_2^{\mathrm{T}} \Lambda_2 [\mathbf{D} - \bar{\mathrm{D}}\,\mathrm{Sgn}(\mathbf{z}_2)] + (\sigma_\theta(\hat{\theta})\hat{\theta}^{\mathrm{T}})\tilde{\theta} \\ \leqslant & -\mathbf{z}_1^{\mathrm{T}} \Lambda_1 C_1 \mathbf{z}_1 - \mathbf{z}_2^{\mathrm{T}} \Lambda_2 C_2 \mathbf{z}_2 \\ \leqslant & -\lambda_{\min}(C_1 \Lambda_1)\|\mathbf{z}_1\|^2 - \lambda_{\min}(C_2 \Lambda_2)\|\mathbf{z}_2\|^2 \\ \leqslant & 0 \end{aligned} \tag{21}$$

where $\lambda_{\min}(\cdot)$ denotes the minimum eigenvalue of a matrix. Since V_3 is a non-negative function and its time derivative is negative semi-definite, V_3 is ensured to be bounded. In addition, we conclude by applying the LaSalle–Yoshizawa theorem [10] to Eq. (21) that $\mathbf{z}_1(t)$, $\mathbf{z}_2(t) \to 0$ as $t \to \infty$. Thus, the position and velocity errors are proven to be globally asymptotically

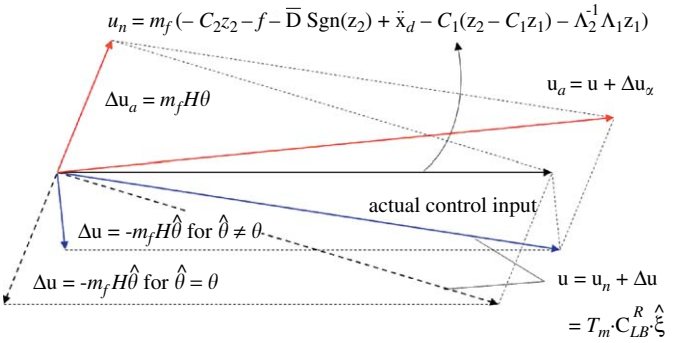

Fig. 2. Schematic illustration of the actual control input and actual thrust force applied to the follower satellite by thrust misalignment.

convergent such that

$$\lim_{t\to\infty} \mathbf{z}_1(t) = 0 \to \lim_{t\to\infty} \mathbf{x}_1(t) - \mathbf{x}_d(t) = 0$$

$$\lim_{t\to\infty} \mathbf{z}_2(t) = 0 \to \lim_{t\to\infty} \mathbf{x}_2(t) - \dot{\mathbf{x}}_d(t) - C_1\mathbf{z}_1(t) = 0$$
$$\to \lim_{t\to\infty} \mathbf{x}_2(t) - \dot{\mathbf{x}}_d(t) = 0 \qquad (22)$$

The boundedness of V_3 implies that $\tilde{\theta}(t)$ is bounded. From the definition of $\tilde{\theta} = \theta - \hat{\theta}$, $\hat{\theta}(t)$ is surely bounded because the unknown parameter θ is a constant. These properties including Eq. (22), along with the assumption of boundedness of $\ddot{\mathbf{x}}_d(t)$, imply that the control input $\mathbf{u}(t)$ is also bounded. Even though the tracking error converges to zero, the estimated misalignment parameter may not converge to its true value. As usual in an adaptive control, persistent excitation (PE) condition should be satisfied in order to attain convergence of the estimated parameter to its true value [15]. However, the above stability and convergence properties can be guaranteed without PE condition.

3.3. Computation of control input

From the definition of $\mathbf{u}(t)$ and $H(t)$ in Eqs. (6) and (8), they include the variables such as the thrust magnitude T_m and the rotation matrix C_{LB}^R. Thus, the control input of Eq. (16) obtained from adaptive backstepping technique cannot be evaluated explicitly because it contains matrix of $H(t)$ including T_m and C_{LB}^R even though system states and design parameters are known except for $H(t)$. So it is necessary to compute the control input by using an alternative approach. One feasible approach is to find the thrust magnitude T_m and matrix C_{LB}^R which satisfy Eq. (16), and then to compute the control input directly from them. After substituting the definition of $\mathbf{u}(t)$ in Eq. (6) and $H(t)$ in Eq. (8) into Eq. (16), we can rewrite Eq. (16) in a simple form

$$\begin{aligned} &T_m \cdot C_{LB}^R \cdot \hat{\xi} = \mathbf{q} - T_m \cdot C_{LB}^R \cdot G \cdot \hat{\theta} \\ &T_m \cdot C_{LB}^R \cdot (\hat{\xi} + G \cdot \hat{\theta}) = \mathbf{q} \\ &T_m \cdot C_{LB}^R \cdot \mathbf{p} = \mathbf{q} \end{aligned} \qquad (23)$$

where

$$\mathbf{p} = \hat{\xi} + G \cdot \hat{\theta}$$

$$\mathbf{q} = m_f(-C_2\mathbf{z}_2 - f - \bar{\mathrm{D}}\,\mathrm{Sgn}(\mathbf{z}_2) + \ddot{\mathbf{x}}_d - C_1(\mathbf{z}_2 - C_1\mathbf{z}_1) - \Lambda_2^{-1}\Lambda_1\mathbf{z}_1)$$

Note that $\hat{\xi} \in R^3$ and $G \in R^{3\times 2}$ are constant vector and matrix related to thrust orientation information, respectively, and $\mathbf{p} \in R^3$, $\mathbf{q} \in R^3$ can be computed directly because their variables are already known or assigned. The thrust magnitude T_m can be obtained simply by using $T_m = (\|\mathbf{q}\|/\|\mathbf{p}\|)$, and the rotation matrix C_{LB}^R can also be constructed by applying the conditions of minimal and optimal proper pointing which produce a unique rotation matrix [16]. Thus, the actual control inputs can be constructed simply by using $\mathbf{u}(t) = T_m \cdot C_{LB}^R \cdot \hat{\xi}$. Note that the actual control input, i.e., the nominal thrust force $\mathbf{u}$, is generated to point thruster toward a proper direction considering compensation of thrust misalignment so that the follower satellite tracks a desired trajectory well. In other words, the last term of the nominal thrust force in Eq. (16) is added to compensate the third term $(H(t)\theta)$ in the second equation of Eq. (8). In actual maneuvers, the control input applied to the follower satellite comprises the thrust magnitude T_m and the attitude control for proper orientation by C_{LB}^R, but the actual force $\mathbf{u}_a$ acting on follower satellite is expressed as the sum of the actual control inputs $\mathbf{u}$ and $\Delta\mathbf{u}_a$ due to the true thrust misalignment. Fig. 2 illustrates the actual force $\mathbf{u}_a$, the actual control input $\mathbf{u}$, and the perturbed forces $\Delta\mathbf{u}$ and $\Delta\mathbf{u}_a$ by the estimated and true thrust misalignment. The nominal control input $\mathbf{u}_n$ shown in Fig. 2 means the first term including

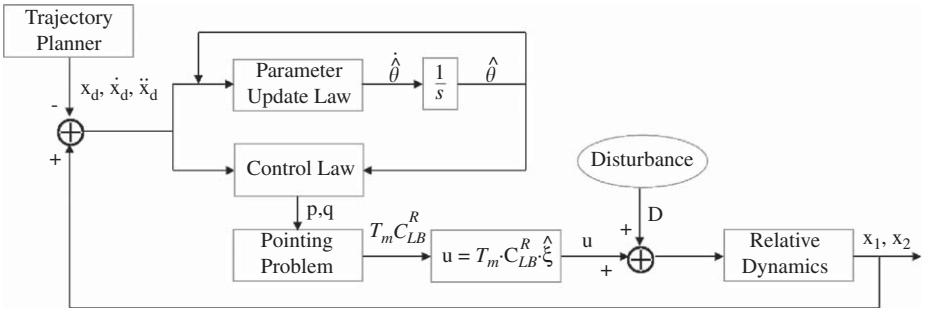

Fig. 3. Overall block diagram of control scheme.

Table 1
Additional parameters for numerical simulations.

Initial conditions	$\mathbf{x}_1(0) = [50, -50, -30]^{\mathrm{T}}$ m, $\dot{\mathbf{x}}_1(0) = [0, 0, 0]^{\mathrm{T}}$ m/s^2 $\hat{\theta}(0) = [0, 0]^{\mathrm{T}}$ deg
Thruster information	$[\alpha, \beta]^{\mathrm{T}} = [210, 210]^{\mathrm{T}}$ deg, $[\Delta\beta, \Delta\alpha]^{\mathrm{T}} = [-1.5, 1.5]^{\mathrm{T}}$ deg
Design parameters	$C_1 = C_2 = 1.0 \times 10^{-3} \times I_{3\times3}$, $\Gamma = 2.0 \times 10^{-3} \times I_{2\times2}$ $\Lambda_1 = 1.0 \times 10^{-2} \times I_{3\times3}$, $\Lambda_2 = 1.0 \times 10^{3} \times I_{3\times3}$
Others	$m_f = 100$ kg, $\bar{\mathrm{D}} = 5 \times 10^{-5}$ N $X_1 = [-100, 100, 100]^{\mathrm{T}} m$, $a = 0.01$, $T_s = 3600$ s

brackets in Eq. (16). It is also obvious that the actual control input $\mathbf{u}$ is equivalent to the actual force $\mathbf{u}_a$ when the estimated parameters from an adaptive control law converge to true values.

Since a single thruster is fixed to a satellite, it is necessary to slew the satellite prior to each burn such that the thruster is pointed toward desired direction by the attitude maneuver. In practical implementation, the proper attitude orientation for thruster burn can be obtained from the rotation matrix C_{LB}^R which is achieved by attitude maneuver. In this study, it is assumed that attitude maneuver is executed by an inner control loop which makes a thruster point to the control direction in real-time without much time delay. In the case of a satellite with 10 kg m^2 of moment of inertia and 25 N m of maximum torque, it is estimated to take 0.23 s for 1° attitude maneuver and 0.52 s for 5° [17]. As obtained in the next simulation, the maximum angle of attitude maneuver in the LVLH frame is smaller than 0.6° for 1 Hz operational frequency and 0.04° for 10 Hz. The control schematic including the computational process of the control input and parameter estimate is illustrated in Fig. 3.

4. Numerical simulations

The adaptive backstepping control law designed in the previous section is simulated for a tracking problem with the following orbital parameters of a leader satellite, $\hat{p}_e = 600$ km, $\hat{e} = 0.2$, and $\hat{n} = 7.75 \times 10^{-4}$, where $\hat{p}_e$ is perigee altitude, $\hat{e}$ is eccentricity of the elliptical orbit, $\hat{n}$ denotes mean motion from which the orbital period can be determined. The desired trajectory and external disturbance are described by

$$\mathbf{x}_d(t) = a \int_0^t e^{-a(t-\tau)} Q_d(\tau)\, d\tau$$
$$\mathbf{d}(t) = [1.9106 - 1.906 - 1.517]^{\mathrm{T}} \sin(2\pi\hat{n}t) \times 10^{-5}\ \mathrm{m/s^2} \tag{24}$$

where

$$Q_d(t) = \begin{cases} \dfrac{X_1}{2} + \dfrac{X_1}{2} \sin\left(\pi\left(\dfrac{t}{T_s} - \dfrac{1}{2}\right)\right), & 0 \leqslant t \leqslant T_s \\ X_1, & t \geqslant T_s \end{cases}$$

The setting time T_s indicates how fast the follower satellite reaches the X_1 position in the desired trajectory. The orbital parameters, desired trajectory and external disturbance are chosen as the same values in Pongvthithum [4]. $\kappa(t)$ in Eq. (5) is given as a small positive random variable within 5×10^{-4} such that it realizes thrust magnitude error in practical maneuvers. Note that the total disturbance is the sum of disturbance caused by thrust magnitude error and external disturbance including the Earth's oblateness, solar radiation pressure, atmospheric drag, third body gravity and electromagnetic force. Additional parameters used for simulation are listed in Table 1. The design parameters were tuned by trial and

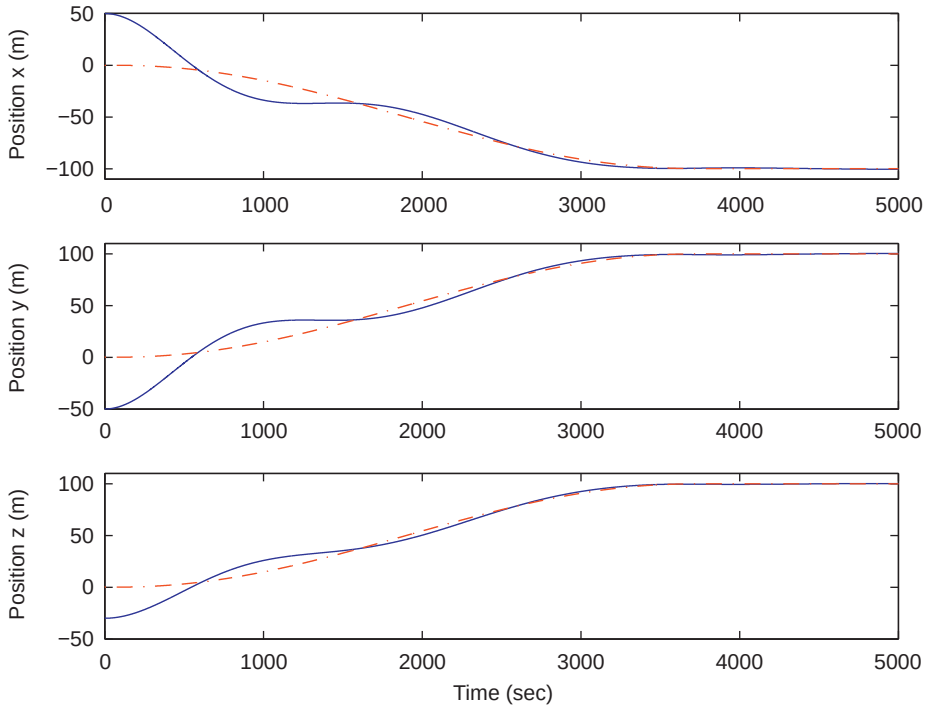

Fig. 4. Real (solid line) and desired (dash-dot line) trajectory of the follower satellite.

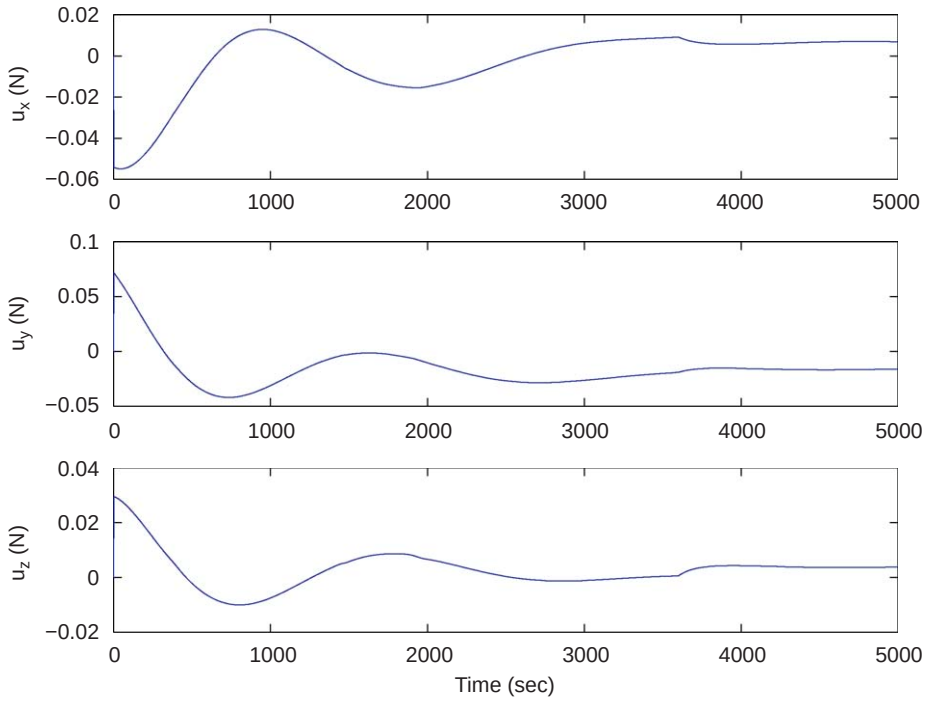

Fig. 5. Actual control input of the follower satellite.

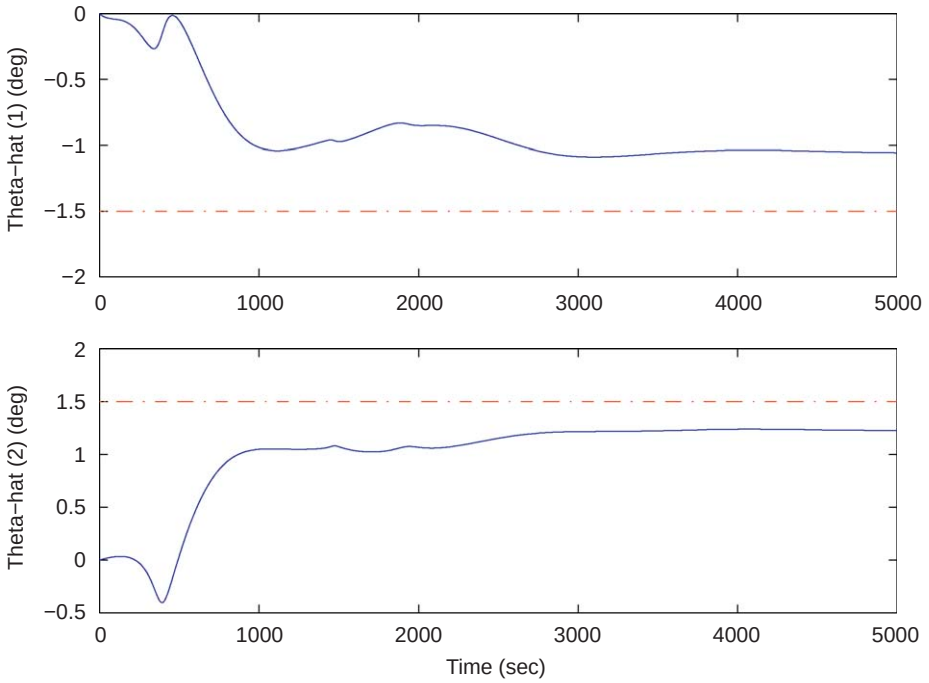

Fig. 6. Estimated (solid line) and real (dash-dot line) values of thrust misalignment.

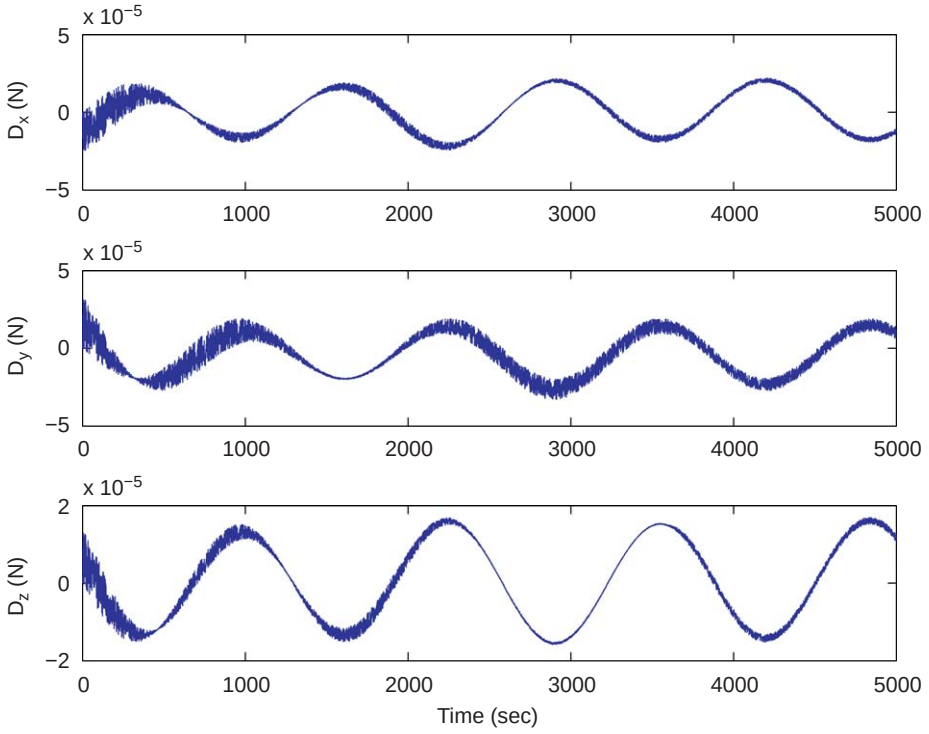

Fig. 7. Total disturbance including external disturbance and thrust magnitude error.

error until the controller and update law shows satisfactory performance considering an admissible thrust magnitude and convergence of the estimated parameters. Other parameters such as initial conditions are selected arbitrarily but the thrust misalignment angles, $\Delta\alpha$ and $\Delta\beta$ are chosen such that they correspond to the statements of Wolff [13].

The simulation results depicted in Figs. 4, 5 and 6 show that the follower satellite tracks the desired trajectory well, and the control inputs are kept small within the range of electric thrusters, and the estimated misalignment converges to an admissible level even though it does not converge to the true value. As shown in Eq. (17), the estimated parameters converge to any values without more update when $\mathbf{z}_2$ and T_m approach zero. For the estimated parameters to converge to their true values, PE condition should be satisfied [15]. The total disturbance including thrust magnitude error is shown in Fig. 7. To demonstrate how the proposed controller is effective for the aspect of fuel consumption, two simulation results are presented in Table 2. Case A shows corresponding fuel cost in terms of ΔV for the proposed adaptive controller considering thrust misalignment as the estimated parameters, and Case B for the backstepping controller regarding it as disturbance. Under the same simulation conditions, $\Delta V = 1.2778\,\mathrm{m/s}$ of Case A is smaller than Case B with difference of $\Delta V = 0.0052\,\mathrm{m/s}$ in 5000 s because perturbation caused by thrust misalignment is compensated by the proposed controller. Fig. 8 shows the thrust forces, $\Delta\mathbf{u}$ and $\Delta\mathbf{u}_a$ of Fig. 2, caused by the estimated and real thrust misalignment, respectively. Their forces approach zero because thrust magnitude decreases as time passes as shown in Fig. 5, and their difference also becomes smaller because the estimated parameters converge to the vicinity of their true values.

5. Conclusions

In this paper, we developed the error model of thrust misalignment, and designed an adaptive control law for

Table 2
Comparison of fuel cost during formation maneuver.

	Time (s)				
	1000	2000	3000	4000	5000
Case A (m/s)	0.4661	0.6288	0.8832	1.0974	1.2778
Case B (m/s)	0.4675	0.6305	0.8899	1.1026	1.2830

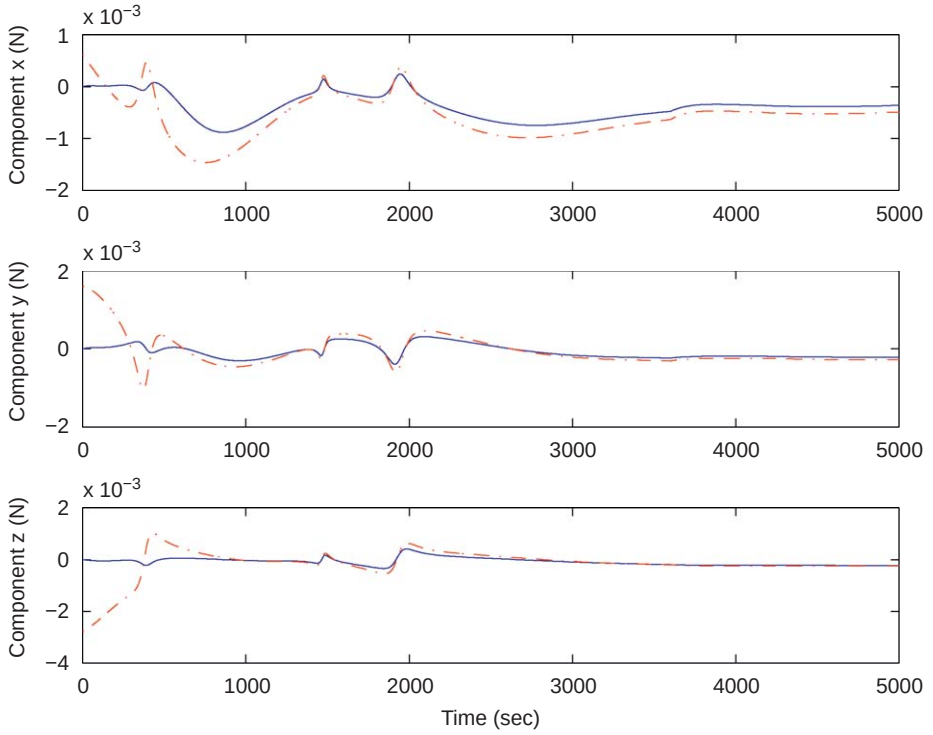

Fig. 8. Thrust force caused by the estimated (solid line) and real (dash-dot line) misalignment.

the tracking problem of SFF under uncertainty of thrust misalignment and bounded disturbances. It was proven by using Lyapunov stability analysis that the proposed controller guarantees global asymptotic convergence for the position and velocity tracking errors. Simulation results were provided to demonstrate the performance of the proposed control law. Compared to a general controller considering thrust misalignment as disturbance, it was shown that the proposed adaptive controller is more efficient in terms of fuel consumption during formation maneuver in the presence of thrust misalignment.

Acknowledgment

This work was supported by Grant no. R01-2006-000-10189-0 from the Basic Research Program of the Korea Science and Engineering Foundation.

References

[1] W.H. Clohessy, R.S. Wiltshire, Terminal guidance system for satellite rendezvous, Journal of the Aerospace Sciences 27 (9) (1960) 653–658.

[2] M.S. de Queiroz, V. Kapila, Q. Yan, Adaptive nonlinear control of multiple spacecraft formation flying, Journal of Guidance, Control, and Dynamics 23 (3) (2000) 385–390.

[3] P. Gurfil, M. Idan, N.J. Kasdin, Adaptive neural control of deep-space formation flying, Journal of Guidance, Control, and Dynamics 26 (3) (2003) 491–501.

[4] R. Pongvthithum, S.M. Veres, S.B. Gabriel, E. Rogers, Universal adaptive control of satellite formation flying, International Journal of Control 78 (1) (2005) 45–52.

[5] H. Wong, V. Kapila, A.G. Sparks, Adaptive output feedback tracking control of spacecraft formation, International Journal of Robust and Nonlinear Control 12 (2002) 117–139.

[6] H. Lim, H. Bang, B. Kim, Adaptive backstepping control for satellite formation flying with thruster error, in: Proceedings of 57th International Astronautical Congress, Valencia, Spain, October 2006, IAC-06-C1.7.02.

[7] I. Kanellakopoulos, P.V. Kokotovic, A.S. Morse, Systematic design of adaptive controllers for feedback linearizable systems, IEEE Transactions on Automatic Control 36 (11) (1991) 1241–1253.

[8] F. Ikhouane, M. Krstic, Robustness of the tuning functions adaptive backstepping design for linear systems, IEEE Transactions on Automatic Control 43 (3) (1998) 431–437.

[9] K.S. Narendra, A.M. Annaswanny, Stable Adaptive Systems, Prentice-Hall, Englewood Cliffs, NY, 1989.

[10] M. Krstic, I. Kanellakopoulos, P. Kokotovic, Nonlinear and Adaptive Control Design, Wiley, New York, 1995.

[11] M. Qingsong, W. Pengji, Y. Di, Low-thrust fuzzy formation keeping for multiple spacecraft flying, Acta Astronautica 55 (11) (2004) 895–901.

[12] L. Hui, L. Junfeng, H. Baoyin, Sliding mode control for low-thrust Earth-orbiting spacecraft formation maneuvering, Aerospace Science and Technology 10 (77) (2006) 636–643.

[13] P.J. Wolff, B.G. Williams, R.M. Vaughan, Navigation considerations for low-thrust planetary missions, in: AAS/AIAA Spaceflight Mechanics Meeting, Monterey, CA, USA, February 1999, AAS 98-201.

[14] H. Wong, H. Pan, M.S. de Queiroz, V. Kapila, Adaptive learning control for spacecraft formation flying, in: Proceedings of 40th IEEE Conference on Decision and Control, Orlando, FL, USA, December 2001, pp. 1089–1094.

[15] J.E. Slotine, W. Li, Applied Nonlinear Control, Prentice-Hall, Englewood Cliffs, NY, 1991.

[16] I.Y. Bar-Itzhack, D. Hershkowitz, L. Rodman, Pointing in real euclidean space, Journal of Guidance, Control and Dynamics 20 (5) (1997) 916–922.

[17] J.L. Junkins, M.R. Akella, R. Robinett, Nonlinear adaptive control of spacecraft maneuvers, Journal of Guidance, Control and Dynamics 20 (6) (1997) 1104–1110.